This manuscript was accepted by J. Chem. Phys. Click here to see the version of record.

# Ultraviolet Relaxation Dynamics in Uracil: Time-resolved Photoion Yield Studies Using a Laser-based Thermal Desorption Source

Omair Ghafur[1,†], Stuart W. Crane[1,†], Michal Ryszka[2], Jana Bockova[2], Andre Rebelo[2,3], Lisa Saalbach[1], Simone De Camillis[4], Jason B. Greenwood[4], Samuel Eden[2,*] and Dave Townsend[1,5,*]

[1] *Institute of Photonics & Quantum Sciences, Heriot-Watt University, Edinburgh, EH14 4AS, United Kingdom*

[2] *School of Physical Sciences, The Open University, Walton Hall, Milton Keynes, MK7 6AA, United Kingdom*

[3] *CEFITEC, Departamento de Física, FCT - Universidade NOVA de Lisboa, P-2829-516 Caparica, Portugal*

[4] *School of Mathematics and Physics, Queen's University Belfast, Belfast BT7 1NN, United Kingdom*

[5] *Institute of Chemical Sciences, Heriot-Watt University, Edinburgh, EH14 4AS, United Kingdom*

## Abstract

Wavelength-dependent measurements of the RNA base uracil, undertaken with nanosecond ultraviolet laser pulses, have previously identified a fragment at *m/z* = 84 (corresponding to the $C_3H_4N_2O^+$ ion) at excitation wavelengths ≤232 nm. This has been interpreted as a possible signature of a theoretically predicted ultrafast ring-opening occurring on a neutral excited state potential energy surface. To further investigate the dynamics of this mechanism, and also the non-adiabatic dynamics operating more generally in uracil, we have used a newly-built ultra-high vacuum spectrometer incorporating a laser-based thermal desorption source to perform time-resolved ion-yield measurements at pump wavelengths of 267 nm, 220 nm and 200 nm. We also report complementary data obtained for the related species 2-thiouracil following 267 nm excitation. Where direct comparisons can be made (267 nm), our findings are in good agreement with previously reported measurements conducted on these systems using cold molecular beams, demonstrating that the role of initial internal energy on the excited state dynamics is negligible. Our 220 nm and 200 nm data also represent the first reported ultrafast study of uracil at pump wavelengths <250 nm, revealing extremely rapid (<200 fs) relaxation of the bright $S_3(^1\pi\pi^*)$ state. These measurements do not, however, provide any evidence for the appearance of the *m/z* = 84 fragment within the first few hundred picoseconds following excitation. This key finding indicates that the detection of this specific species in previous nanosecond work is not directly related to an ultrafast ring opening process. An alternative excited state process, operating on a more extended timescale, remains an open possibility.



* Corresponding authors: E-mail d.townsend@hw.ac.uk, s.p.eden@open.ac.uk

† These authors contributed equally to this work.

## I. INTRODUCTION

Over the past two decades the relaxation dynamics of electronically excited DNA and RNA nucleobases following ultraviolet (UV) irradiation have attracted considerable attention.[1-5] This has largely been motivated by a desire to better understand various photochemical/photophysical pathways that potentially damage living organisms (through the formation of lesions in critical macromolecules) or, alternatively, provide rapid and efficient routes for the harmless dissipation of excess energy (so-called "photo-protection" mechanisms). Many experimental studies have focused on isolated species in the gas phase, providing an instructive "bottom up" starting point for developing detailed insight into such pathways, free from perturbations due to the surrounding environment (e.g. solvation and/or clustering effects). This approach also provides benchmarks for complimentary *ab initio* theoretical studies undertaken with high-level computational chemistry methodologies able to capture the dynamics of decay pathways.

Based on the above rationale, the pyrimidine RNA base uracil has been the subject of numerous gas-phase spectroscopy and dynamics studies across the ~220-270 nm UV absorption region.[6-15] This sizable body of work, supported by extensive theoretical input,[16-30] has started to reveal a complex picture of competing non-radiative decay pathways occurring on femtosecond to nanosecond timescales. These include internal conversion (IC) from the optically prepared $S_2(^1\pi\pi^*)$ state direct to the $S_0$ ground state and also IC from $S_2(^1\pi\pi^*)$ to the lower-lying $S_1(^1n\pi^*)$ state, which can then subsequently relax to $S_0$ or, alternatively, undergo intersystem crossing to the triplet manifold. A more detailed overview of the substantial literature describing these various processes is omitted here in the interests of brevity. The reader is, however, directed to the work of Richter *et al*. for a more expanded perspective, which includes instructive graphical summaries of the various relaxation schemes proposed to date.[17] At this point, we limit our outline to briefly

highlighting theoretically predicted ultrafast (i.e. sub-picosecond) excited-state ring-opening mechanisms which served as the initial motivation behind this present study. Ring-opening channels would potentially have destabilizing effects, acting in competition with photo-protective decay routes leading ultimately back to the ground electronic state. Nachtigallová *et al.*[18] described an $S_2/S_1$ ring-opening conical intersection (CI) and predicted this would lead to new photochemical products. Richter *et al*.,[17] also carried out dynamical calculations with non-adiabatic and spin-orbit couplings and reported an $S_1/S_0$ ring-opening CI. Similarly, Nachtigallová *et al.* reported an $S_1/S_0$ ring-opening CI but discussed it in much less detail than the $S_2/S_1$ pathway. All of these CIs involve ring-opening via cleavage of the $N_3$-$C_4$ bond (see Fig. 1). Some supporting experimental evidence for a ring opening pathway (as a minor decay channel) has been previously suggested in studies by Barc *et al*., [9] where multiphoton ionization of uracil was investigated over the 220-270 nm region using a nanosecond laser. Here the observation of $m/z$ = 84 fragment ions at wavelengths ≤232 nm was proposed to arise as a consequence of the $S_2/S_1$ ring-opening CI. This fragment was identified as $C_3H_4N_2O^+$ in subsequent measurements using deuterated uracil[31] and, critically, is absent in single-photon ionization or collision experiments involving direct access to excited ionic states.[32] Depending on the calculation method, the energies of all three predicted ring-opening CIs are energetically consistent with the experimental onset of $C_3H_4N_2O^+$ production.[17, 18] Moreover, $N_3$-$C_4$ ring-opening leaves a CO group exposed at one end of the molecule and the loss of this moiety following photoionization would yield the observed $C_3H_4N_2O^+$ fragment. In view of this intriguing result, we have conducted a series of exploratory time-resolved ion-yield (TRIY) measurements on uracil in an attempt to further characterize the origin of this specific fragmentation pathway. Although TRIY measurements often lack mechanistic sensitivity when compared to more differential time-resolved photoelectron spectroscopy/imaging methodologies,

they are ideally suited to this specific propose. Pump excitation wavelengths of 267 nm, 220 nm and 200 nm were employed in conjunction with an intense 400 nm probe. The pump at 220 nm and 200 nm increases the range of radiationless deactivation pathways when compared with previous ultrafast experiments (250-267 nm),[6, 8, 10, 13-15] including possible access to theoretically-predicted ring-opening processes. It also provides the first time-resolved experimental study of relaxation in the $S_3(^1\pi\pi^*)$ state, which is at least as bright as $S_2(^1\pi\pi^*)$ but has been investigated in far less depth. Our work also makes use of a laser-based thermal desorption strategy to introduce a gas-phase plume of uracil directly into the pump-probe interaction region. In order to provide an additional benchmark for this approach – the results from which may be compared to previous studies using more conventional molecular beam methods – we also investigated the related species 2-thiouracil using a 267 nm pump. This provides insight into the influence of initial temperature on key electronic excited state dynamics.

## II. EXPERIMENTAL

Time-resolved experiments were conducted using a newly-built ultra-high vacuum spectrometer dedicated to the study of non-volatile species. As illustrated schematically in Fig. 2, the instrument consists of a standard CF160 6-way cross (evacuated by a 300 l/s turbomolecular pump) and a flight tube extension arm consisting of a CF63 cube and CF63 4-way cross (connected to a 60 l/s turbomolecular pump). This is terminated by a 40 mm dual micro-channel plate (MCP)/P47 phosphor screen detector assembly. A support flange with a 22 mm diameter hole provides moderate differential pumping between the detector and interaction chambers, and also supports a set of ion accelerating electrodes. These electrodes incorporate a laser-based thermal desorption source for producing gas-phase samples of neutral non-volatile molecules, based on the

design of Greenwood and co-workers.[33, 34] The source consists of a piece of 10 μm thick 316 stainless steel foil (Ø = 16 mm) on which uracil or 2-thiouracil powder (Sigma-Aldrich, ≥99% purity) was deposited using application of methanol to ensure a uniform coating 300-500 μm thick. The loaded foil was then clamped within the repeller electrode, positioning the sample ~2.5 mm from the pump-probe interaction region. Production of gas-phase species was accomplished by irradiating the rear (i.e. uncoated) side of the foil with the focused output of a CW laser diode (Kale CNC), producing a maximum of ~1 W at 445 nm. The relatively low thermal conductivity of stainless steel, together with the thinness of the foil, ensures that laser light absorption results in a localized hot-spot from which molecules undergo thermal desorption. The temperature and area of this spot was controlled by adjusting the voltage supplied to the diode and/or by adjusting the focusing conditions. These parameters were typically set to produce a laser power of ~330 mW and a spot on the foil ~1 mm in diameter. This produced a localized estimated foil temperature of ~420 ± 30 K (see Appendix A) which is not sufficient to induce thermal decomposition of the uracil/2-thiouracil samples and yields only the lowest energy diketo and oxo-thione tautomers illustrated in Fig. 1. Our approach, based on low-cost, readily available diode lasers that can be easily coupled into vacuum through a window, is straightforward, economical and easily controllable. A potential drawback, however, is that the analyte deposited on the foil is depleted during the measurement, at the point where the CW laser induces thermal desorption. In order to greatly extend periods of uninterrupted data acquisition, the center of the circular foil on which sample is deposited is displaced from the central time-of-flight axis running along the instrument (see inset within Fig. 2). Rotation of this foil within the repeller electrode assembly therefore permits the sample to be periodically replenished. Typically this was performed every 45-60

minutes, when data acquisition was temporarily suspended following completion of a full pump-probe delay scan.

Charged species produced at the region of interaction between the desorbed sample molecules and the pump/probe laser pulses are accelerated along the flight tube towards the MCP by the electrode assembly. The resulting light emitted from the phosphor screen was then detected by a fast silicon photomultiplier (SensL, MicroFm-100350X18/MicroEVB-1mm) positioned external to the vacuum. Simulations of the overall electrode configuration design (conducted using SIMION 8.0) were optimized to permit full velocity-map imaging[35] and DC slice imaging[36] of charged species. The instrument therefore has additional capability beyond that employed in the present TRIY measurements and data from experiments utilizing this will be reported in due course.

The laser employed for the TRIY experiments was a 3.8 W, 1 kHz, regeneratively amplified Ti:Sapphire system (Spectra-Physics, Spitfire Pro/Empower) seeded by a Ti:Sapphire oscillator (Spectra-Physics, Tsunami/Millennia). Pump-probe measurements were performed by dividing the 800 nm central wavelength output with multiple beamsplitters and passing one of the resulting beams (to be used for generation of the probe) off a gold retroreflector mounted on a computer-controlled linear translation stage (Physik Instrumente, M-403.12S). UV light at 267, 220 and 200 nm was employed to photoexcite the desorbed uracil molecules and 400 nm light was used as the probe. The 267 nm (~1.6 μJ/pulse) and 200 nm (~0.2 μJ/pulse) pump beams were the third and fourth harmonics of the starting 800 nm beam, respectively, generated in a multi-stage delay line set-up using thin β-barium borate (BBO) crystals. To obtain 220 nm pulses, the 1258 nm signal beam output of an optical parametric amplifier (Spectra Physics, OPA-800C) was mixed

with 800 nm to produce visible light at 489 nm. This was then combined with an additional 400 nm pulse to generate ~0.3 μJ/pulse of 220 nm by sum-frequency generation. Once again, BBO provided the non-linear medium in the various stages of this process. Finally, the intense 400 nm probe used in all measurements (~20 μJ/pulse, ~$2 \times 10^{12}$ W/cm$^2$ when focused) was produced by frequency doubling a separate portion of 800 nm output from the laser amplifier. The pump and probe beams had parallel polarizations directed perpendicular to the spectrometer time-of-flight axis and were collinearly combined using a thin dichroic mirror before entering the spectrometer via a 1 mm thick $CaF_2$ window. For 220/200 nm excitation, pump and probe focusing was achieved independently (i.e. pre-combination) via fused silica ($f$ = 50 cm) and calcium fluoride ($f$ = 63 cm) plano-convex lenses, respectively. When performing 267 nm excitation, the pump and probe were focused post-combination using a 50 cm focal length UV enhanced concave aluminium mirror.

At each pump-probe delay, the output of the photomultiplier was recorded by an oscilloscope interfaced to a PC running custom data acquisition code written in MATLAB. This code also controlled homemade shutters that were used for automated recording of pump-alone and probe-alone background signals at each pump-probe time-step. Data collection runs scanned the translation stage repeatedly over a series of small linear increments at short pump-probe delay times and larger, exponentially increasing steps to sample more extended system dynamics. Specific details are provided within the various figure captions. Temporal experimental resolution was determined by backfilling the interaction chamber with diethlyether using a leak valve and recording non-resonant multiphoton ionization cross-correlation measurements of its parent ion. Numerical cross-correlation values obtained were 140 ± 10 fs, 175 ± 15 fs and 170 ± 15 fs when using the 267 nm, 220 nm and 200 nm pump wavelengths, respectively. Given the similar

This manuscript was accepted by J. Chem. Phys. Click here to see the version of record.

ionization potentials of diethylether (vertical ~9.5 eV)[37, 38] and uracil (vertical ~9.6 eV, adiabatic 9.34 eV)[39, 40] the parent ion signals from both molecules originate predominantly from the same photon order process at all pump wavelengths investigated. Although the ionization potential of 2-thiouracil is considerably lower (vertical 8.80 eV),[41] the ionization photon order is the same as diethylether for the case of a 267 nm pump wavelength, which was the only one used with this system.

## III. RESULTS & DISCUSSION

### A. 267 nm Excitation: Uracil and 2-Thiouracil Parent Ion Transients

Benchmarking TRIY measurements were undertaken on both uracil and 2-thiouracil, at an excitation wavelength of 267 nm. Here initial excitation is almost exclusively to the $S_2(^1\pi\pi^*)$ state. Energetically, this is below the previously reported threshold for potentially observing the *m/z* = 84 fragment in uracil, but provides direct comparisons with previous studies conducted at or near this excitation energy using more conventional molecular beam methods.[6, 8, 10, 11, 13-15, 42] Transient mass-spectra are shown in Fig. 3. Cuts though this data at pump-probe delay times of $\Delta t = 0$ and 5 ps, along with the time-invariant pump-alone and probe-alone fragment distributions, are presented in Fig. 4. For uracil, we obtained a fragmentation pattern with 4 main peaks at *m/z* = 112 (the parent ion), 69 ($C_3H_3NO^+$), 42/41 ($C_2H_2O^+$ plus others) and 28 ($CH_2N^+$). This is in good agreement with previously reported data acquired using range of different techniques including electron impact ionization[40, 43-46], proton impact ionization[44, 47, 48], one-color single- and multi-photon ionization[9, 31, 32] and a series of time-resolved studies by Weinacht and co-workers employing an intense 780 nm ionizing probe in conjunction with resonant 260 nm excitation.[8, 10, 11, 49] A somewhat less intense peak at *m/z* = 14 (predominantly $CH_2^+$) was also observed, as were

This manuscript was accepted by J. Chem. Phys. Click here to see the version of record.

extremely weak features at *m/z* = 53/54, 26, and 1. These observations indicate our present measurements exhibit good overall detection sensitivity (for example, the weak *m/z* = 26 ion channel was not discernable above the background noise in a number of previous mass spectrometry studies[47]). The assignment of specific fragment masses is discussed in detail elsewhere.[9, 31] In 2-thiouracil, a larger number of ion peaks were observed (see Fig. 4), including strong features at *m/z* = 128 (parent ion), 69, 42/41 and 28.

In order to undertake quantitative analysis of the excited state dynamics, we first consider the parent ion transients obtained as a function of the pump-probe delay $\Delta t$. We employed a sequential Levenberg-Marquardt data fitting routine wherein the transient ionization signals $S(\Delta t)$ are described as:

$$S(\Delta t) = \sum_{i=1}^{n} P_i(\Delta t) \otimes g(\Delta t) \qquad (1)$$

Here $g(\Delta t)$ denotes the experimentally determined Gaussian cross-correlation and the series of $n$ exponentially decaying functions $P_i(\Delta t)$, each with an associated fit amplitude $a_i$, are defined as follows:

$$P_i(\Delta t) = a_i \exp[-\Delta t / \tau_i] \qquad (i = 1)$$
$$P_i(\Delta t) = a_i \exp[-\Delta t / \tau_i]\left(1 - \exp[-\Delta t / \tau_{i-1}]\right) \qquad (i > 1) \qquad (2)$$

Three exponentially decaying functions evolving in the positive (pump-probe) time direction were required to satisfactorily fit the parent ion data for both uracil and 2-thiouracil. This effectively represents a sequential A $\rightarrow$ B $\rightarrow$ C $\rightarrow$ D model for the dynamics where A denotes the state prepared in the initial optical excitation while B - D are populations prepared subsequently via non-radiative processes. Additionally, a single exponential function evolving extremely rapidly in the negative time direction was also included. The requirement for such a "probe-pump"

component is not surprising as both uracil and 2-thiouracil absorb very strongly at 200 nm (equivalent to 2-photon absorption of the intense 400 nm probe). We label the various exponential fit functions using their respective time constants $\tau_{-1}$ (probe-pump) and $\tau_{1-3}$ (pump-probe).

Fig. 5 presents the application of the overall fitting analysis described above to the parent ion data shown in Fig. 3. In uracil, the longest time constant $\tau_3$ = 3.0 ± 0.5 ps agrees well with temporal signatures seen in several previous TRIY studies employing similar excitation wavelengths in conjunction with multi-photon probes.[8, 10, 15] These studies generally agree on an initial <100 fs ultrafast decay, followed by a longer lifetime of between 2.2-3.2 ps. An outlier is the study of Canuel *et al.*,[13] which observed decays of 130 fs and 1.1 ps. Overall, the longer time constant has been also confirmed by a recent time-resolved photoelectron spectroscopy (TRPES) study from Ullrich and co-workers,[6] which reported a dynamical signature exhibiting a 2.35 ± 0.47 ps 1/*e* lifetime. This more differential measurement (relative to TRIY) employed pump excitation at 260 nm in conjunction with a two-photon 290 nm probe and, based upon observed changes in photoelectron binding energies, also reported a value of ~170 fs for the shorter time-constant. This is longer than that seen in the previous TRIY studies, which may be rationalized by the possibility of coherent processes occurring at time-zero when employing intense multi-photon probes.[15] Analysis of our present data requires two rapidly decaying functions to fit the short-time pump-probe dynamics accurately, $\tau_1$ ~ Gaussian and $\tau_2$ = 200 ± 20 fs, perhaps reflecting elements of two distinct process that have not always been fully distinguishable in some previous measurements. The excellent signal-to-noise in this data means we can be confident that two short time constants are required in the fitting procedure.

Although we note that other mechanistic schemes have also been proposed,[17] in keeping broadly with the interpretation presented by Ullrich and co-workers[6] we assign the physical origin

This manuscript was accepted by J. Chem. Phys. Click here to see the version of record.

of our Gaussian $\tau_1$ feature to extremely rapid relaxation of the initially prepared $S_2(^1\pi\pi^*)$ state towards its minimum energy geometry (with some fraction of population also possibly decaying directly to $S_0$). The slightly longer dynamical feature $\tau_2 = 200 \pm 30$ fs then describes the subsequent internal conversion of (geometry relaxed) $S_2(^1\pi\pi^*)$ to the lower-lying $S_1(^1n\pi^*)$ state, the decay of which is modelled by $\tau_3 = 3.0 \pm 0.5$ ps. A critical additional result here is that the overall dynamics and associated time constants we observe using our laser-based desorption approach are very similar to those reported using molecular beam methods. This suggests thermal excitation in low-frequency (<500 $cm^{-1}$) out-of-plane bending vibrations of the aromatic ring system[50, 51] does not exert significant influence on the dynamical timescales and mechanisms operating in uracil at this excitation energy. Although out-of-plane modes have been implicated as critical in accessing conical intersections mediating the electronically excited state dynamics, our observations confirm that access to conical intersections connecting $S_2(^1\pi\pi^*)$ to lower lying electronic states is essentially barrierless. [17, 19, 20, 22, 27]

The aforementioned uracil TRPES study by Ullrich and co-workers also reported a long-lived component exhibiting a lifetime >1 ns – assigned to the triplet manifold populated via intersystem crossing from the $S_1(^1n\pi^*)$ state. The absence of such a feature in our parent ion data is attributed to our two photon probe energy (6.2 eV) being somewhat less than in this earlier investigation (8.4 eV). We therefore do not project sufficiently deeply into the ionization continuum to efficiently pick up this additional, long-lived feature – as confirmed by the previously reported electron binding energy spectrum.[6] Helpfully, this observation leads us to conclude that 1 + 3′ ionization using our 400 nm probe is either (i) not a significant factor in our present parent ion measurements or (ii) leaves the parent ion so internally excited that it rapidly fragments with

This manuscript was accepted by J. Chem. Phys. Click here to see the version of record.

a probability close to unity. In either case, the parent ion signals we detect here must therefore originate predominantly from 1+2′ ionization.

In 2-thiouracil, we note that our parent ion time constants of $\tau_1 = 50 \pm 20$ fs, $\tau_2 = 310 \pm 30$ fs, and $\tau_3 = 90 \pm 20$ ps are, as was the case in uracil, in excellent agreement with a very recently reported TRPES study that investigated a range of pump wavelengths spanning 292-249 nm (notably $\tau_1 < 50$ fs, $\tau_2 = 333$ fs, and $\tau_3 = 109$ ps at 271 nm excitation). Once again, this work was undertaken by Ullrich and co-workers,[42] and we follow these authors in assigning $\tau_1$ to the decay of the initially excited $S_2(^1\pi\pi^*)$ state to $S_1(^1n\pi^*)$, $\tau_2$ to modelling ultrafast intersystem crossing to the triplet manifold and $\tau_3$ then capturing the decay of the lowest energy triplet state back to the $S_0$ electronic ground state. This overall pathway is also broadly consistent with recent theoretical predictions.[52] In contrast to uracil, our two photon probe scheme (total 6.2 eV) is now able to pick up the longer-lived triplet state dynamics operating in 2-thiouracil due its significantly (~0.8 eV) lower ionization potential. We are now able to project sufficiently deeply into the ionization continuum to efficiently detect the triplet state manifold. As with uracil, the similarity of our numerical time constants to those obtained under colder target conditions suggests that the internal energy imparted in our laser-based thermal desorption approach is not sufficient to significantly modify the relaxation dynamics probed here. This is a potentially important finding as it helps strengthen analogies with biological environments drawn from cold molecular beam experiments on uracil and its analogues.

### C. 267 nm Excitation: Uracil and 2-Thiouracil Fragment Ion Transients

Individual fragment ion transients obtained from uracil following 267 nm excitation are presented in Fig. 6 for *m/z* = 69, 42/41, 28 and 14. All fragments display broadly similar temporal

evolution, but Fig. 3 and Fig. 5 clearly reveal this is distinctly different from the parent ion. In particular, much longer-lived dynamical processes are seen, extending well beyond the 25 ps pump-probe delay range sampled. This even includes a slight rise in signal level beyond ~8 ps. A similar situation is also observed in 2-thiouracil (see Fig. 3). It is initially tempting to assume these observations provide additional information relating to the dynamics operating in the neutral excited states of these systems. This could be in the form of higher-order (i.e. 1 + 3′) multiphoton ionization efficiently probing low-lying, but vibrationally excited states in the parent (thereby producing highly internally excited cations which readily fragment) or, alternatively, multiphoton ionization of photofragments formed following dissociation of the neutral parent species. The caveat here, however, is that the temporal evolution of fragment ions seen in our data may also be induced via independent dynamical processes operating solely in the parent cation. This may occur when ionization is achieved exclusively via the 267 nm pump beam and prepares excited ionic states that evolve dynamically on different timescales to those populated in the neutral species. Subsequent photoabsorption at 400 nm then probes these cation dynamics by inducing additional, prompt fragmentation. The overall temporal evolution of the fragment ion pump-probe transients we observe in our data may therefore be a superposition of multiple unconnected processes involving both neutral and cation dynamics. Reliable deconvolution and analysis of such data therefore becomes impossible within the one-dimensional measurement framework of a TRIY experiment. This appears to be confirmed by several pieces of supporting evidence, as discussed in Appendix B. As such, we are not able to consider the transient behavior of the fragments further. We note that non-adiabatic relaxation dynamics have recently been investigated theoretically in the uracil cation and these studies predict extremely rapid internal conversion to the $D_0$ ground state occurs before significant fragmentation takes place.[53, 54]

### D. 220 nm and 200 nm Excitation: Uracil Parent Ion Transients

We now consider uracil excitation at shorter wavelengths. As discussed in the Introduction, observing the time-resolved appearance of a fragment ion at *m/z* = 84 would provide corroborating evidence for the existence of an ultrafast ring-opening pathway. Initial investigations employed a 220/400 nm pump-probe combination – a choice guided by the study of Barc *et al.*,[9] who reported the greatest abundance of this specific fragment at 220 nm using nanosecond multiphoton ionization (the shortest excitation wavelength employed in that work). As evident from the transient data presented in Figs 7 and 8, however, our measurements did not provide evidence for the appearance of any new fragments (when compared to 267 nm excitation) on the <1 ps timescale predicted by dynamical simulations.[17, 18] As illustrated in previous measurements with higher mass resolution,[9, 31] the peaks we do observe have a finer substructure that we cannot discern (due to the >100 ns decay time of the phosphor screen, which obscures closely spaced features). Nonetheless, the absence of any strong ion signals in the *m/z* =80-90 region means we should easily be able to observe a new peak appearing at *m/z* = 84, if it was present at these excitation energies. Our contrast should also be satisfactory, especially since the *m/z* = 84 fragment is produced by two photon absorption at 220 nm[9] (i.e. it should also be observable via 1 + 2′ ionization in our 220/400 nm pump/probe measurement and not require a 1 + 3′ process). Even at much more extended pump-probe delays out to 100 ps (the limit of our translation stage) and at ~330 ps in a fixed-delay measurement, we failed to observe evidence of any fragments other than those seen following 267 nm excitation.

As the measurements of Barc *et al.* reported an onset for *m/z* = 84 production at close to 232 nm, with a steadily increasing contribution up to 220 nm, it was deemed plausible that the

This manuscript was accepted by J. Chem. Phys. Click here to see the version of record.

relative size of this fragment signal may continue to increase as the excitation wavelength is further shortened. Moreover, based upon the vapor-phase absorption spectrum of uracil,[55] the appearance of the *m/z* = 84 fragment may, in fact, be associated in some way with the second strong ππ* absorption band of uracil – denoted here as $S_3(^1\pi\pi^*)$ – which starts to supersede the $S_2(^1\pi\pi^*)$ band at ~220 nm and peaks at 190 nm. We therefore also performed TRIY measurements at a pump wavelength of 200 nm (Fig. 7 and 8), but again our scans failed to find any evidence for a peak at *m/z* = 84 up to a pump-probe delay of 10 ps.

Despite seeing no evidence of an ultrafast ring-opening pathway, the time-resolved behavior of the *m/z* = 112 parent ion is still of interest as our data are the first reported pump-probe measurements in uracil at excitation wavelengths <250 nm. Temporal analysis was conducted using the same procedure as described earlier, but now only three exponential functions (including one going backwards to account for probe-pump signals) were required to produce a satisfactory fit. A very small constant baseline offset was also included in the model to account for imperfect subtraction of pump-alone and probe-alone signals in this data. The outcome is shown in Fig. 9. For the case of both 220 nm and 200 nm excitation, the observable dynamics only persist for a fraction of a picosecond, displaying an effectively Gaussian $\tau_1$ component and a much smaller amplitude feature exhibiting $\tau_2$ of 190-200 fs. This is in marked contrast to the more extended lifetimes seen with the 267 nm pump. The excellent agreement between the fitted time constants extracted from our 267 nm benchmarking data and previously reported experimental measurements does, however, reinforce confidence in the shorter pump wavelength analysis.

Theoretical work has suggested that direct excitation to the $S_3(^1\pi\pi^*)$ state proceeds via extremely rapid internal conversion to $S_2(^1\pi\pi^*)$.[17] From this point the relaxation then proceeds in a similar manner to longer excitation wavelengths, with $S_2(^1\pi\pi^*)$ population passing through the

This manuscript was accepted by J. Chem. Phys. Click here to see the version of record.

$S_1(^1n\pi^*)$ state en route to $S_0$ or the triplet manifold. At 220 nm, excitation is expected to populate both the $S_2(^1\pi\pi^*)$ and $S_3(^1\pi\pi^*)$ states to some extent, whereas population will almost exclusively be prepared in $S_3(^1\pi\pi^*)$ at 200 nm.[55] The very similar dynamics we observe at both pump wavelengths therefore suggests that decay of the $S_3(^1\pi\pi^*)$ state is extremely rapid (i.e. not resolvable within our current measurement) and that the $S_2(^1\pi\pi^*)$ state is also extremely short-lived. Our parent ion measurements alone, however, are not able to reveal if the observed transients also reflect an extremely rapid decay of the subsequently populated $S_1(^1n\pi^*)$ state as well. This is expected to be significantly faster than the 3.0 ps seen following 267 nm excitation. On the other hand, poor Franck-Condon factors for efficient ionization of highly vibrationally excited $S_1(^1n\pi^*)$ may mean we are now effectively blind to this state at the total pump + probe energies used. Alternatively, following ionization from highly vibrationally excited $S_1(^1n\pi^*)$, the parent ion is likely to dissociate extremely readily, meaning it will not be detected in our time-of-flight measurement. The ~200 fs decay seen in the parent transient data may therefore only reflect the $S_2(^1\pi\pi^*)$ lifetime. The challenges in fitting fragment ion decay curves due to the potential contributions of ionic state dynamics (see Section III C) mean that the time-dependence of fragment ion production at these shorter wavelengths does not provide any reliable additional insight here. This is especially true since, as seen in Fig 7, the dynamics operating in the $m/z$ = 69 channel are not consistent with $m/z$ = 42/41 and 28, with the former exhibiting somewhat more rapid overall decay. As such, our data only permit us to place an upper bound on the $S_2(^1\pi\pi^*)$ lifetime of ~200 fs here.

### E. Nanosecond Studies Revisited

The dynamical timescales seen in our present laser-based thermal desorption work following 267 nm excitation in uracil and 2-thiouracil are in good agreement with previously reported cold molecular beam studies. Even so, since the original nanosecond studies reporting the $m/z = 84$ ion were conducted under molecular beam conditions, thermal effects may still potentially be a factor in the failure to observe this fragment in our TRIY data. To investigate this possibility further, the nanosecond measurements were repeated at the Open University (OU) using the same instrument employed in the original report[9] but with the supersonic molecular beam nozzle replaced by a laser-based thermal desorption source similar to that used in the TRIY study. The only difference of note was that the OU source does not enable foil rotation, reducing the experimental time available for each preparation of the uracil sample. A more detailed description will be provided in a forthcoming publication.

Results for 220 nm multiphoton ionization with nanosecond pulses are shown in Fig. 10. The $m/z = 84$ fragment is clearly apparent, providing conclusive evidence that elevated sample temperature is not responsible for the lack of observed $m/z = 84$ signal in the TRIY measurements. It is interesting to note, however, that the overall fragmentation pattern in Fig. 10 is quite different to that seen in Fig. 7. In particular, the nanosecond data exhibits a significantly smaller feature at $m/z = 69$ when compared to the TRIY case. This could potentially be explained by the higher (0.56 – 1.13 eV) total photon energy leading to increased fragmentation in the TRIY measurements (see Table I), although similar discrepancies also arise when the total photon energy is identical. This is clear, for example, when comparing our uracil 267 nm pump only data in Fig. 4 with the 266 nm multiphoton ionization mass spectrum reported previously.[9] Making meaningful comparisons in terms of total absorbed energy is challenging, however, as both sets of measurements contain

different combinations of ionization schemes associated with the various product ions. Previous studies making direct comparisons between (pump-only) femtosecond and nanosecond ionization have also reported significant differences in ion production patterns, with femtosecond pulses typically inducing less overall fragmentation. This has been rationalized by considering differing propensities for "ladder-climbing" vs "ladder-switching" ionization processes as the laser pulse duration changes.[56-60] In the former, photon absorption occurs exclusively in the parent species from which all smaller fragments originate (either directly or indirectly). In the latter, photon absorption may also occur in the fragment ions, inducing further dissociation. Ladder-switching behaviour is expected to become more likely with longer pulses since fragmentation of the parent occurs within the laser pulse duration. When compared to pump-alone femtosecond ionization, the pump-probe nature of a TRIY measurement effectively enhances the ladder-switching pathway (i.e. delay of the probe with respect to the pump increases the likelihood of any probe absorption by fragments). Even so, the range of delays sampled in our present measurements (100 ps) is still extremely small relative to the 7 ns pulses used in the original multiphoton ionization experiments of Barc *et al.*.[9] Invoking a ladder-switching ionization process as a possible source of $m/z$ = 84 fragments in the nanosecond measurements is unsatisfactory here however, as this requires a minimum of three 220 nm photons to be absorbed. As mentioned earlier, previous power dependence studies have shown this fragment only needs two such photons to facilitate its production.[9] This suggests that dynamics operating in neutral uracil on a longer timescale than that sampled in the present TRIY measurements may be responsible for the formation of the $m/z$ = 84 species. Obvious candidates for this are long-lived triplet states.

This manuscript was accepted by J. Chem. Phys. Click here to see the version of record.

## IV. CONCLUSION

We have presented the first results from a newly constructed spectrometer that employs a laser-based thermal desorption source for the gas-phase study of low-vapor pressure molecular samples. Time-resolved ion-yield measurements have been conducted on the isolated RNA base uracil at pump wavelengths of 267 nm, 220 nm and 200 nm, in conjunction with a 400 nm multiphoton probe. Complementary data are also reported for 267 nm excitation of the related species 2-thiouracil. The 267 nm findings are in good agreement with previously reported time-resolved measurements conducted at similar excitation wavelengths on these molecules, providing useful benchmarking for the new instrument. The data obtained following 220 nm and 200 nm excitation represent the first reported ultrafast study of uracil at pump wavelengths <250 nm. Extremely rapid relaxation to the $S_3(^1\pi\pi^*)$ state is observed in <200 fs. The key finding, however, is that our measurements do not provide any evidence for the appearance of $m/z$ = 84 fragment ions within the first few hundred picoseconds of pump-probe delay. This suggests detection of this specific species in previous nanosecond work cannot be directly linked to ultrafast ring opening processes predicted theoretically at $S_2/S_1$ or $S_1/S_0$ conical intersections. On the other hand, an alternative excited state process operating on a much more extended timescale remains an open possibility and an interesting avenue for future investigation.



## ACKNOWLEDGEMENTS

This work was supported by Leverhulme Trust Research Project Grant RPG-2012-735, Carnegie Trust Research Incentive Grant 70264 and financial support from Engineering and Physical Sciences Research Council (EPSRC) Grant EP/P001459/1. S.E. also acknowledges support from EPSRC Grants EP/E039618/1, EP/J002577/1 and EP/L002191/1. The PhD studies

of J.B. and A.R are funded by the Open University and the Radiation Biology and Biophysics (RaBBIT) doctoral training programme of the Universidade NOVA de Lisboa (PD/00193/2012, PD/BD/114449/2016). Heriot-Watt University are also acknowledged for providing S.W.C. and L.S. with PhD funding support.

## APPENDIX A. Characterization of Desorption Source

Before undertaking TRIY measurements it was important to (i) confirm no thermal decomposition takes place prior to photoionization and (ii) consider the internal temperature of the samples prepared by our laser-based desorption process. The former was achieved by observing the ratio of fragment to parent ions produced over a range of desorption laser power settings using one-color multi-photon ionization at 267 nm (see Section III C for a more expanded discussion of the fragments observed). As seen in Fig. A1, this ratio remains unchanged for all major ion fragments produced from uracil – a strong indicator that no significant thermal decomposition is induced by the desorption laser itself over the range of settings sampled. To estimate the localized temperature to which the stainless steel substrate foil is heated by the desorption laser under specific power and focusing conditions, a K-type (chromel–alumel) thermocouple contact was placed at the centre of the ~1 mm beam focus. The thermal conductivities of both chromel (~18 W $m^{-1}$ $K^{-1}$) and alumel (~30 W $m^{-1}$ $K^{-1}$) are very low[61] and similar to stainless steel (~16 W $m^{-1}$ $K^{-1}$).[62] Furthermore, the reflectivities of chromel and alumel (both >90% nickel) are also expected to be comparable to that of steel at the 445 nm desorption laser wavelength (for a similar surface finish quality, which we assume to be reasonable here).[63] This approach therefore permits a rudimentary estimation of the foil substrate temperature and, as seen in Fig. A1, this is predicted to be ~420 ± 30 K in our present time-resolved measurements. This also places an upper limit on

This manuscript was accepted by J. Chem. Phys. Click here to see the version of record.

the temperature of the desorbed molecular sample. Corroborating the information from our fragment ratio data, such a temperature would seem insufficient to induce significant thermal decomposition in chemically stable species such as uracil and 2-thiouracil. Furthermore, we highlight that the same thermal desorption approach has been used previously to introduce the much more thermally unstable DNA nucleosides into the gas-phase intact.[64] An additional point to consider is that both molecules exhibit various tautomeric forms in addition to the di-keto (uracil) and oxo-thione (2-thiouracil) structures shown in Fig. 1. Calculations on both systems have shown, however, that all such additional tautomers lie >1500 $cm^{-1}$ above the diketo and oxo-thione species.[65-67] At temperatures in the region of 420 K (and even some way above this), these various tautomers will not therefore be present in our desorbed sample plume to any significant extent.

## APPENDIX B. Cation Dynamics in Fragment Ion Transients

Three independent pieces of initial evidence lead us to suggest that cation dynamics may play a non-negligible role in the observed uracil fragment ion transients; (i) None of the fragment peaks show any discernable offset in appearance time relative to the parent. This observation would seem to rule out ionization of neutral photofragments since two uracil ring bonds need to be broken to form all of the species we observe and our experimental time resolution should therefore be able to discern their nascent formation. Furthermore, it has been previously suggested[32, 46, 49] that formation of $m/z$ = 42/41 and 28 fragments occurs sequentially via $m/z$ = 69; (ii) Attempts to fit the data using a number of different models (sequential and/or parallel) with various numbers of exponential functions were unable to extract numerical time constants similar to those seen in the parent. This is an important consideration as, if the fragment transients only provide signatures of neutral dynamics, they should accurately reflect the time constants seen in

This manuscript was accepted by J. Chem. Phys. Click here to see the version of record.

the parent ion in addition to other, longer lived processes; (iii) Data from several experimental reports[32, 40, 44] and also a theoretical study specifically considering photoionization via the $S_2(^1\pi\pi^*)$ state[49] reveal that the energetic appearance thresholds for various uracil fragments require (at least) a 1 + 3′ ionization process in our present experiment (see Table I). The large relative magnitude of the fragment peaks (especially near $\Delta t = 0$) compared to that of the parent – which we have already established arises predominantly from a 1+2′ process – would therefore seem to suggest 1 + 3′ ionization is not exclusively producing these fragments. An additional contribution from lower probe photon order processes is likely to also be occurring (e.g., one-photon 400 nm probe absorption by the uracil parent cation following direct three-photon ionization by the pump).

To further investigate the role of competing neutral vs. cation dynamics in our uracil fragment ion transients, a series of power dependence measurements were conducted to determine the ionizing photon order of the probe. This was performed for the fragments $m/z$ = 69, 42/41, 28 and 14 at pump-probe delays of $\Delta t$ = 0 and 5 ps, and also for the parent ion $m/z$ = 112 at $\Delta t$ = 0 (no measurement was possible at 5 ps due to lack of signal). The 400 nm probe power was varied between 4 and 10 μJ/pulse (to avoid the saturation regime) and background signals originating from 267 nm pump-only and 400 nm probe-only ionization were subtracted from the total recorded ion signal. We estimate the number of probe photons absorbed ($\alpha_{probe}$) using the equation $I = cP^{\alpha_{Probe}}$, where $I$ is ion intensity, $c$ is a constant, and $P$ is the 400 nm photon fluence. Plotting the probe laser power *vs.* pump-probe ion signal on logarithmic scales then yields a straight line where the gradient gives the probe photon order (see Fig. B2). For the parent ion, $\alpha_{probe}$ is 1.7, which is close to the expected integer value of 2. At $\Delta t$ = 0 the power dependence of the various fragments varies between 1.4 ($m/z$ = 69) and 2.1 ($m/z$ = 14). On the basis of the threshold appearance energy data summarized in Table I, these values for $\alpha_{probe}$ are much smaller than would

be anticipated if the fragments originate from dynamical processes associated with neutral species – especially for $m/z$ = 42/41 and 28, where values ≥ 3 would clearly be predicted. This provides a strong indication that cation dynamics (probed with a low 400 nm photon order) are also contributing strongly to the observed fragment signals close to $\Delta t = 0$. Such dynamics appear short-lived, however, as suggested at the more extended pump-probe delay of $\Delta t$ = 5 ps. Here the photon order is clearly seen to increase significantly, spanning the range 2.6-3.2. As evident from Table I, a value of $\alpha_{probe}$ ~3 is more in keeping with fragments being produced following predominantly (1+ 3′) ionization direct from neutral excited states rather than post-ionization via optically induced electronic transitions within the cation. Furthermore, ps-order dynamics exhibited by the fragment transients would be consistent with the timescales seen for the uracil triplet manifold by Ullrich and co-workers in their TRPES data[6], as discussed in the main text. This present analysis supports the overall fragment transients obtained following 267 nm excitation exhibiting a mixture of cation and neutral excited state dynamics that cannot be reliably analyzed quantitatively – particularly at short $\Delta t$. Note that the same issues are also expected to exist in our measurements for fragments produced using 220 nm and 200 nm. Although the pump intensity employed here is almost an order of magnitude lower than at 267 nm, only two pump photons (rather than three) are required to ionize uracil in this instance (see Table I). More generally, however, recording fragment transients with greatly reduced pump power (where all pump-alone ionization is fully suppressed) may offer a route to additional quantitative insight into the neutral excited state dynamics operating in the uracil system. This does, of course, come at the price of dramatically reduced signal-to-noise levels.

## REFERENCES


1 C. E. Crespo-Hernández, B. Cohen, P. M. Hare, and B. Kohler, Chem. Rev. **104**, 1977 (2004).
2 C. T. Middleton, K. de La Harpe, C. Su, Y. K. Law, C. E. Crespo-Hernández, and B. Kohler, Annu. Rev. Phys. Chem. **60**, 217 (2009).
3 L. Serrano-Andrés, and M. Merchán, J. Photoch. Photobio. C **10**, 21 (2009).
4 K. Kleinermanns, D. Nachtigallová, and M. S. de Vries, Int. Rev. Phys. Chem. **32**, 308 (2013).
5 R. Improta, F. Santoro, and L. Blancafort, Chem. Rev. **116**, 3540 (2016).
6 H. Yu, J. A. Sanchez-Rodriguez, M. Pollum, C. E. Crespo-Hernández, S. Mai, P. Marquetand, L. González, and S. Ullrich, Phys. Chem. Chem. Phys. **18**, 20168 (2016).
7 M. Ligare, F. Siouri, O. Bludsky, D. Nachtigallová, and M. S. de Vries, Phys. Chem. Chem. Phys. **17**, 24336 (2015).
8 S. Matsika, M. Spanner, M. Kotur, and T. C. Weinacht, J. Phys. Chem. A **117**, 12796 (2013).
9 B. Barc, M. Ryszka, J. Spurrell, M. Dampc, P. Limão-Vieira, R. Parajuli, N. J. Mason, and S. Eden, J. Chem. Phys. **139**, 244311 (2013).
10 M. Kotur, T. C. Weinacht, C. Zhou, and S. Matsika, IEEE J. Sel. Top. Quant. **18**, 187 (2012).
11 S. Matsika, C. Zhou, M. Kotur, and T. C. Weinacht, Faraday Discuss. **153**, 247 (2011).
12 M. Schneider, C. Schon, I. Fischer, L. Rubio-Lago, and T. Kitsopoulos, Phys. Chem. Chem. Phys. **9**, 6021 (2007).
13 C. Canuel, M. Mons, F. Piuzzi, B. Tardivel, I. Dimicoli, and M. Elhanine, J. Chem. Phys. **122**, 074316 (2005).
14 S. Ullrich, T. Schultz, M. Z. Zgierski, and A. Stolow, Phys. Chem. Chem. Phys. **6**, 2796 (2004).
15 H. Kang, K. T. Lee, B. Jung, Y. J. Ko, and S. K. Kim, J. Am. Chem. Soc. **124**, 12958 (2002).
16 P. Carbonniere, C. Pouchan, and R. Improta, Phys. Chem. Chem. Phys. **17**, 11615 (2015).
17 M. Richter, S. Mai, P. Marquetand, and L. Gonzalez, Phys. Chem. Chem. Phys. **16**, 24423 (2014).
18 D. Nachtigallová, A. J. A. Aquino, J. J. Szymczak, M. Barbatti, P. Hobza, and H. Lischka, J. Phys. Chem. A **115**, 5247 (2011).
19 V. B. Delchev, A. L. Sobolewski, and W. Domcke, Phys. Chem. Chem. Phys. **12**, 5007 (2010).
20 M. Barbatti, A. J. A. Aquino, J. J. Szymczak, D. Nachtigallová, P. Hobza, and H. Lischka, P. Natl. Acad. Sci. USA **107**, 21453 (2010).
21 M. Barbatti, A. J. A. Aquino, and H. Lischka, Phys. Chem. Chem. Phys. **12**, 4959 (2010).
22 Z. Lan, E. Fabiano, and W. Thiel, J. Phys. Chem. B **113**, 3548 (2009).
23 M. Etinski, T. Fleig, and C. A. Marian, J. Phys. Chem. A **113**, 11809 (2009).
24 E. Epifanovsky, K. Kowalski, P.-D. Fan, M. Valiev, S. Matsika, and A. I. Krylov, J. Phys. Chem. A **112**, 9983 (2008).
25 H. R. Hudock, B. G. Levine, A. L. Thompson, H. Satzger, D. Townsend, N. Gador, S. Ullrich, A. Stolow, and T. J. Martinez, J. Phys. Chem. A **111**, 8500 (2007).
26 T. Climent, R. González-Luque, M. Merchán, and L. Serrano-Andrés, Chem. Phys. Lett. **441**, 327 (2007).
27 M. Merchán, R. González-Luque, T. Climent, L. Serrano-Andrés, E. Rodríguez, M. Reguero, and D. Peláez, J. Phys. Chem. B **110**, 26471 (2006).
28 M. Z. Zgierski, S. Patchkovskii, T. Fujiwara, and E. C. Lim, J. Phys. Chem. A **109**, 9384 (2005).
29 S. Matsika, J. Phys. Chem. A **109**, 7538 (2005).
30 S. Matsika, J. Phys. Chem. A **108**, 7584 (2004).

[31] M. Ryszka, R. Pandey, C. Rizk, J. Tabet, B. Barc, M. Dampc, N. J. Mason, and S. Eden, Int. J. Mass Spectrom. **396**, 48 (2016).

[32] H.-W. Jochims, M. Schwell, H. Baumgärtel, and S. Leach, Chem. Phys. **314**, 263 (2005).

[33] C. R. Calvert, L. Belshaw, M. J. Duffy, O. Kelly, R. B. King, A. G. Smyth, T. J. Kelly, J. T. Costello, D. J. Timson, W. A. Bryan, T. Kierspel, P. Rice, I. C. E. Turcu, C. M. Cacho, E. Springate, I. D. Williams, and J. B. Greenwood, Phys. Chem. Chem. Phys. **14**, 6289 (2012).

[34] F. Calegari, A. Trabattoni, A. Palacios, D. Ayuso, M. C. Castrovilli, J. B. Greenwood, P. Decleva, F. Martín, and M. Nisoli, J. Phys. B: At. Mol. OPt. Phys. **49**, 142001 (2016).

[35] A. T. J. B. Eppink, and D. H. Parker, Rev. Sci. Instrum. **68**, 3477 (1997).

[36] D. Townsend, M. P. Minitti, and A. G. Suits, Rev. Sci. Instrum. **74**, 2530 (2003).

[37] B. J. Cocksey, J. H. D. Eland, and C. J. Danby, J. Chem. Soc. B, 790 (1971).

[38] K. Watanabe, J. Chem. Phys **26**, 542 (1957).

[39] K.-W. Choi, J.-H. Lee, and S. K. Kim, Chem. Commun., 78 (2006).

[40] S. Denifl, B. Sonnweber, G. Hanel, P. Scheier, and T. D. Märk, Int. J. Mass Spectrom. **238**, 47 (2004).

[41] A. R. Katritzky, M. Szafran, and G. Pfister-Guillouzo, J. Chem. Soc. Perkin Trans. 2, 871 (1990).

[42] J. A. Sánchez-Rodriguez, A. Mohamadzade, S. Mai, B. Ashwood, M. Pollum, P. Marquetand, L. González, C. E. Crespo-Hernández, and S. Ullrich, Phys. Chem. Chem. Phys. **18**, 19756 (2017).

[43] M. Imhoff, Z. Deng, and M. A. Huels, Int. J. Mass Spectrom. **262**, 154 (2007).

[44] B. Coupier, B. Farizon, M. Farizon, M. J. Gaillard, F. Gobet, N. V. de Castro Faria, G. Jalbert, S. Ouaskit, M. Carré, B. Gstir, G. Hanel, S. Denifl, L. Feketeova, P. Scheier, and T. D. Märk, Eur. Phys. J. D **20**, 459 (2002).

[45] S. M. Hecht, A. S. Gupta, and N. J. Leonard, Biochim. Biophys. Acta **182**, 444 (1969).

[46] J. M. Rice, G. O. Dudek, and M. Barber, J. Am. Chem. Soc. **87**, 4569 (1965).

[47] J. Tabet, S. Eden, S. Feil, H. Abdoul-Carime, B. Farizon, M. Farizon, S. Ouaskit, and T. D. Märk, Phys. Rev. A **81**, 012711 (2010).

[48] A. Le Padellec, P. Moretto-Capelle, M. Richard-Viard, J. P. Champeaux, and P. Cafarelli, J. Phys. Conf. Ser. **101**, 012007 (2008).

[49] C. Zhou, S. Matsika, M. Kotur, and T. C. Weinacht, J. Phys. Chem. A **116**, 9217 (2012).

[50] M. A. Palafox, V. K. Rastogi, R. P. Tanwar, and L. Mittal, Spectrochim. Acta A **59**, 2473 (2003).

[51] C. Puzzarini, M. Biczysko, and V. Barone, J. Chem. Theory Comput. **7**, 3702 (2011).

[52] S. Mai, P. Marquetand, and L. González, J. Phys. Chem. Lett. **7**, 1978 (2016).

[53] M. Assmann, T. Weinacht, and S. Matsika, J. Chem. Phys **144**, 034301 (2016).

[54] M. Assmann, H. Köppel, and S. Matsika, J. Phys. Chem. A **119**, 866 (2015).

[55] L. B. Clark, G. G. Peschel, and I. Tinoco, J. Phys. Chem. **69**, 3615 (1965).

[56] N. P. Lockyer, and J. C. Vickerman, Int. J. Mass Spectrom. **176**, 77 (1998).

[57] J. Matsumoto, C.-H. Lin, and T. Imasaka, Anal. Chim. Acta **343**, 129 (1997).

[58] K. W. D. Ledingham, and R. P. Singhal, Int. J. Mass Spectrom. **163**, 149 (1997).

[59] P. Aicher, U. Wilhelm, and J. Grotemeyer, J. Am. Soc. Mass Spectrom. **6**, 1059 (1995).

[60] R. Weinkauf, P. Aicher, G. Wesley, J. Grotemeyer, and E. W. Schlag, J. Phys. Chem. **98**, 8381 (1994).

[61] B. Sundqvist, J. Appl. Phys. **72**, 539 (1992).

[62] M. J. Assael, and K. Gialou, Int. J. Thermophys. **24**, 1145 (2003).

[63] G. B. Sabine, Phys. Rev. **55**, 1064 (1939).
[64] S. De Camillis, J. Miles, G. Alexander, O. Ghafur, I. D. Williams, D. Townsend, and J. B. Greenwood, Phys. Chem. Chem. Phys. **17**, 23643 (2015).
[65] C. Puzzarini, M. Biczysko, V. Barone, I. Peña, C. Cabezas, and J. L. Alonso, Phys. Chem. Chem. Phys. **15**, 16965 (2013).
[66] B. M. Guiliano, V. Feyer, K. C. Prince, M. Coreno, L. Evangelisti, S. Maelandri, and W. Caminati, J. Phys. Chem. A **114**, 12725 (2010).
[67] J. Rejnek, M. Hanus, M. Kabeláč, F. Ryjáček, and P. Hobza, Phys. Chem. Chem. Phys. **7**, 2006 (2005).

**Table I**

| Fragment (m/z) | App. energy (eV) |
|---|---|
| 112 | 9.34[a] |
| 69 | 10.85-10.87[b] |
| 42/41 | 12.95-13.41[b] |
| 28 | 13.75-13.83[b] |
| 14 | - |

| Ionization process | Total photon energy (eV) |
|---|---|
| 1 × 267 nm + 2 × 400 nm | 10.85 |
| 1 × 267 nm + 3 × 400 nm | 13.95 |
| 2 × 267 nm | 9.30 |
| 3 × 267 nm | 13.95 |
| 1 × 220 nm + 2 × 400 nm | 11.83 |
| 1 × 220 nm + 3 × 400 nm | 14.93 |
| 2 × 220 nm | 11.27 |
| 3 × 220 nm | 16.91 |
| 1 × 200 nm + 2 × 400 nm | 12.40 |
| 1 × 200 nm + 3 × 400 nm | 15.5 |
| 2 × 200 nm | 12.40 |
| 3 × 400 nm | 9.30 |
| 4 × 400 nm | 12.40 |

Table I: Summary of uracil fragment appearance energies and total available energies for various combinations of pump (267/220/200 nm) and probe (400 nm) photons.

[a] Ref 39

[b] Refs 32, 40 & 44

## Figure Captions

**Figure 1.** Schematic structures of the lowest energy tautomers of uracil (diketo form, with ring atom numbering) and 2-thiouracil (oxo-thione form).

**Figure 2.** TRIY spectrometer overview. The rear repeller electrode (A) incorporates a clamp holding a 10 μm stainless steel foil on which sample is deposited before being desorbed using a 445 nm CW diode laser. The foil clamp is located at one end of a larger cylindrical mount, to facilitate easy installation and removal. Circular motion of the rotation coupler is achieved via a mechanical air-to-vacuum feedthrough (not shown), generating counter-rotation of the foil-plus-cylinder arrangement via a simple gear system. A gold brush contact maintains the electrical connection to the repeller electrode at all times (required as the foil holder rotates on Teflon bearings). The ion optics are 80 mm in diameter, mounted on 4 × 10 mm diameter PEEK support rods. Spacing between the outer edges of the electrodes is 8 mm (A-B) or 12 mm (B-E). The extractor electrode (B) consists of a flat plate (1.5 mm thick) with an 8 mm diameter through hole plus an 8 mm thick aperture with a conical taper (26 to 36 mm diameter). Electrodes C-E are 8 mm wide, have an inner lip thickness of 3 mm and 26 mm diameter clear apertures. The overall distance from the pump/probe laser interaction region to the detector is 97 cm. Additional mu-metal shielding (not shown), extending from the bulkhead holding the ion optics to the MCP detector, may also be installed for photoelectron detection measurements (with the CF63 4-way cross removed).

**Figure 3.** TRIY plots for uracil and 2-thiouracil excited at 267 nm and probed by an intense 400 nm pulse. Data collection runs scanned the translation stage repeatedly between -300 fs to +600 fs in 30 fs steps and +600 fs to +25 ps over 9 exponentially increasing increments.

**Figure 4.** Mass spectra obtained for uracil and 2-thiouracil under 267 nm pump-alone, 400 nm probe-alone and two different pump-probe delay time conditions.

**Figure 5.** Parent ion transients obtained from uracil (top) and 2-thiouracil (bottom) following 267/400 nm pump/probe ionization. Also shown are the overall results of the sequential fitting procedure described in the main text, the individual fit components and the associated residuals (i.e., the overall fit subtracted from the raw data).

**Figure 6.** Transients obtained from various uracil fragment ions following 267/400 nm pump/probe ionization. Each plot is normalized to the maximum intensity seen in that specific fragment channel.

**Figure 7.** TRIY plots for uracil excited at 220 nm (top) or 200 nm (bottom) and probed by an intense 400 nm pulse. Data collection runs scanned the translation stage between -330 fs to +1.2 ps in 30 fs steps and +1.2 ps to +100 ps over 59 exponentially increasing increments (220 nm) and between -400 fs to +2450 fs in 30 fs steps and +2450 fs to +10 ps over 59 exponentially increasing increments (200 nm). Following 200 nm excitation there is significantly more fragmentation than at 220 nm.

**Figure 8.** Expanded view of the mass spectra obtained for uracil close to the $m/z$ = 84 region at two selected pump-probe delay times ($\Delta t$ = 0 and $\Delta t$ = 1 ps) following excitation at 220 nm (top) and 200 nm (bottom).

**Figure 9.** Parent ion transients obtained from uracil following 220/400 nm (top) and 200/400 nm (bottom) pump/probe ionization. Also shown are the overall results of the sequential fitting procedure described in the main text, the individual fit components and the associated residuals (i.e., the overall fit subtracted from the raw data).

**Figure 10.** Resonance-enhanced multiphoton ionization mass spectrum obtained from uracil using nanosecond 220 nm laser pulses following gas phase generation using laser-based thermal desorption. A peak at *m/z* = 84 is clearly visible, as observed in previous molecular beam experiments (e.g., see Fig. 3 of Ref. 9). As an aside, we note that the tail feature observed on the *m/z* = 69 peak and the broad peak centred at *m/z* =87.6 are due to metastable HNCO loss from excited uracil ions, as expanded upon in Ref. 9.

**Figure A1.** Ratio of fragment-to-parent ion signals obtained from uracil following 267 nm irradiation when using different desorption laser powers (for fragments *m/z* = 69, 42/41 & 28). The desorption laser was focused to a spot of ~1 mm diameter on the rear side of a stainless steel foil on which the uracil sample was deposited. Also included is the estimated foil temperature (see supporting text for more details). The shaded region indicates operating conditions used in the TRIY measurements. Error bars denote 1σ uncertainties. Horizontal bars represent error in desorption laser power. Corresponding uncertainties in foil temperature are significantly (~3×) larger.

**Figure B1.** Power dependence plots showing the 400 nm ionizing photon order ($\alpha_{probe}$) for the uracil parent ion (*m/z* = 112) and various fragment ions at 0 ps and 5 ps pump-probe delay.

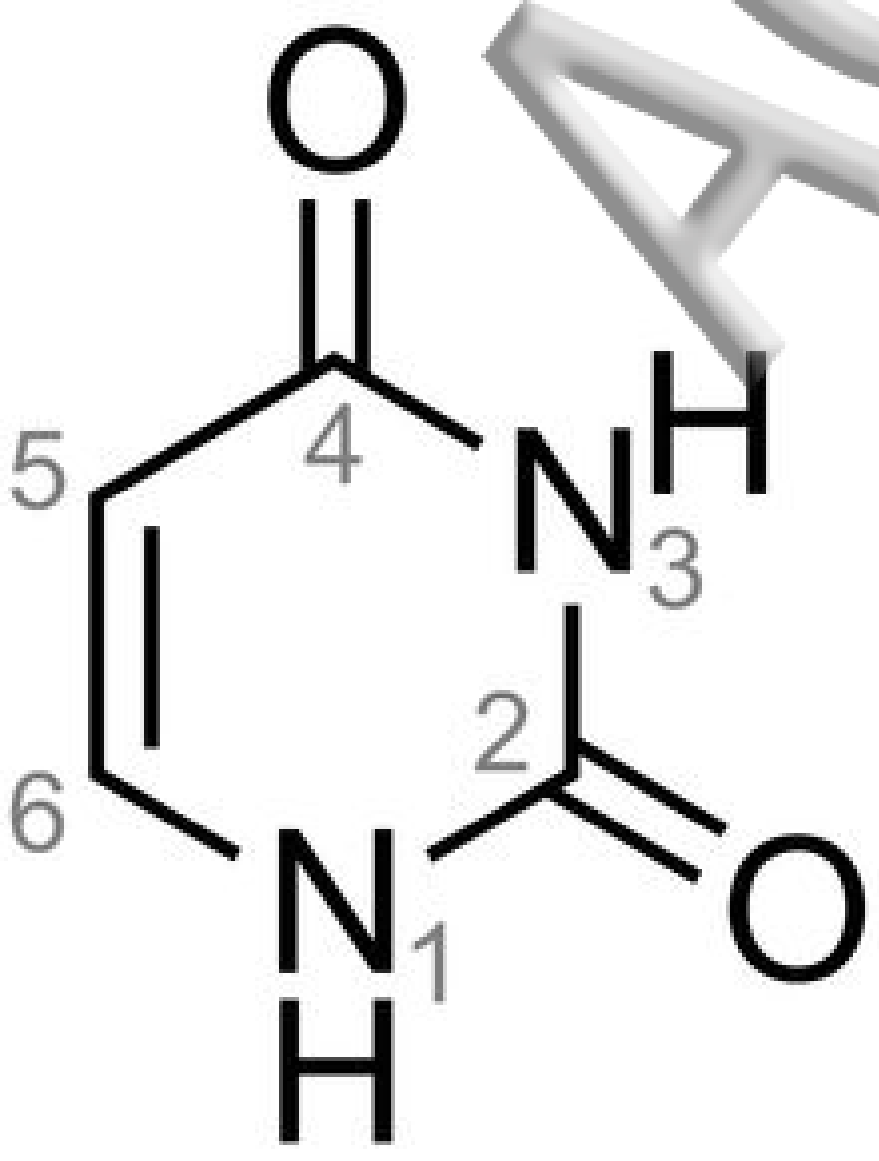


Uracil

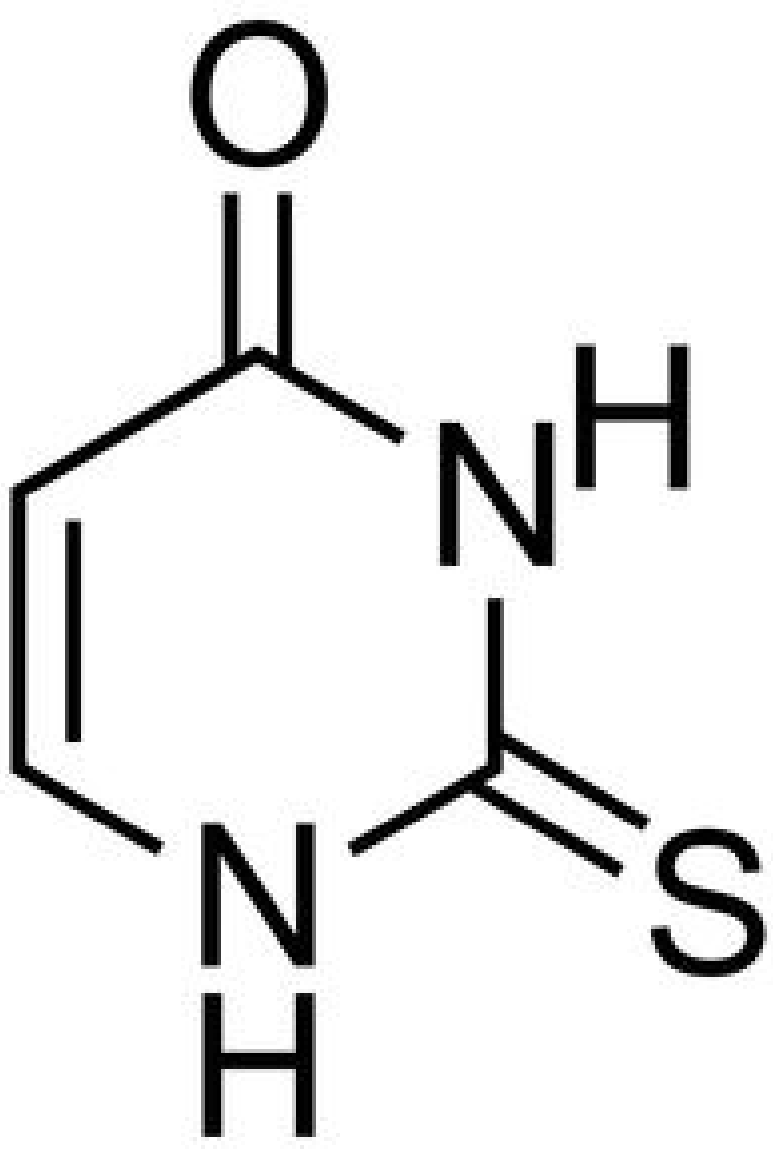


2-Thiouracil

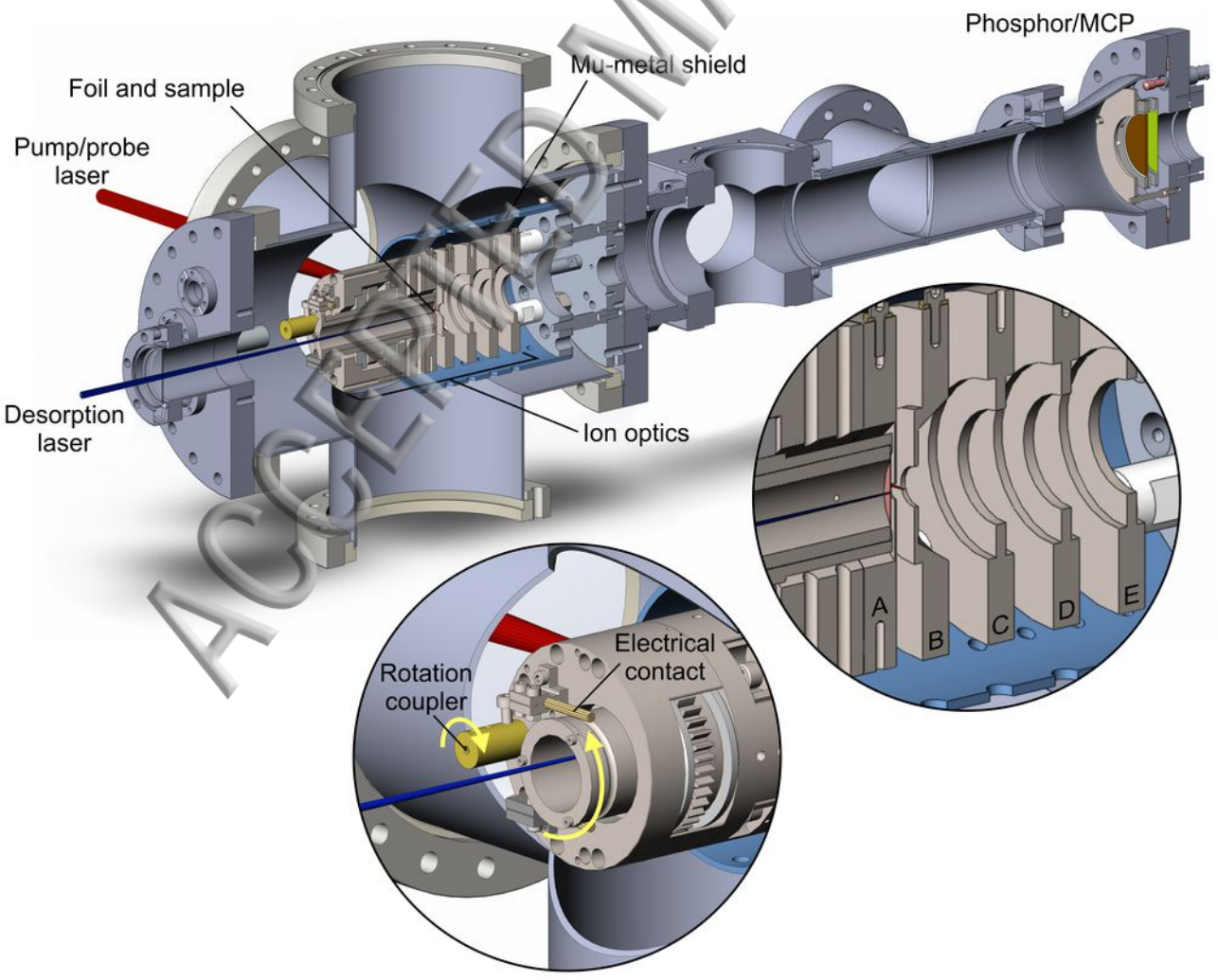
Phosphor/MCP
Mu-metal shield
Foil and sample
Pump/probe laser
Desorption laser
Ion optics
A
B
C
D
E
Rotation coupler
Electrical contact

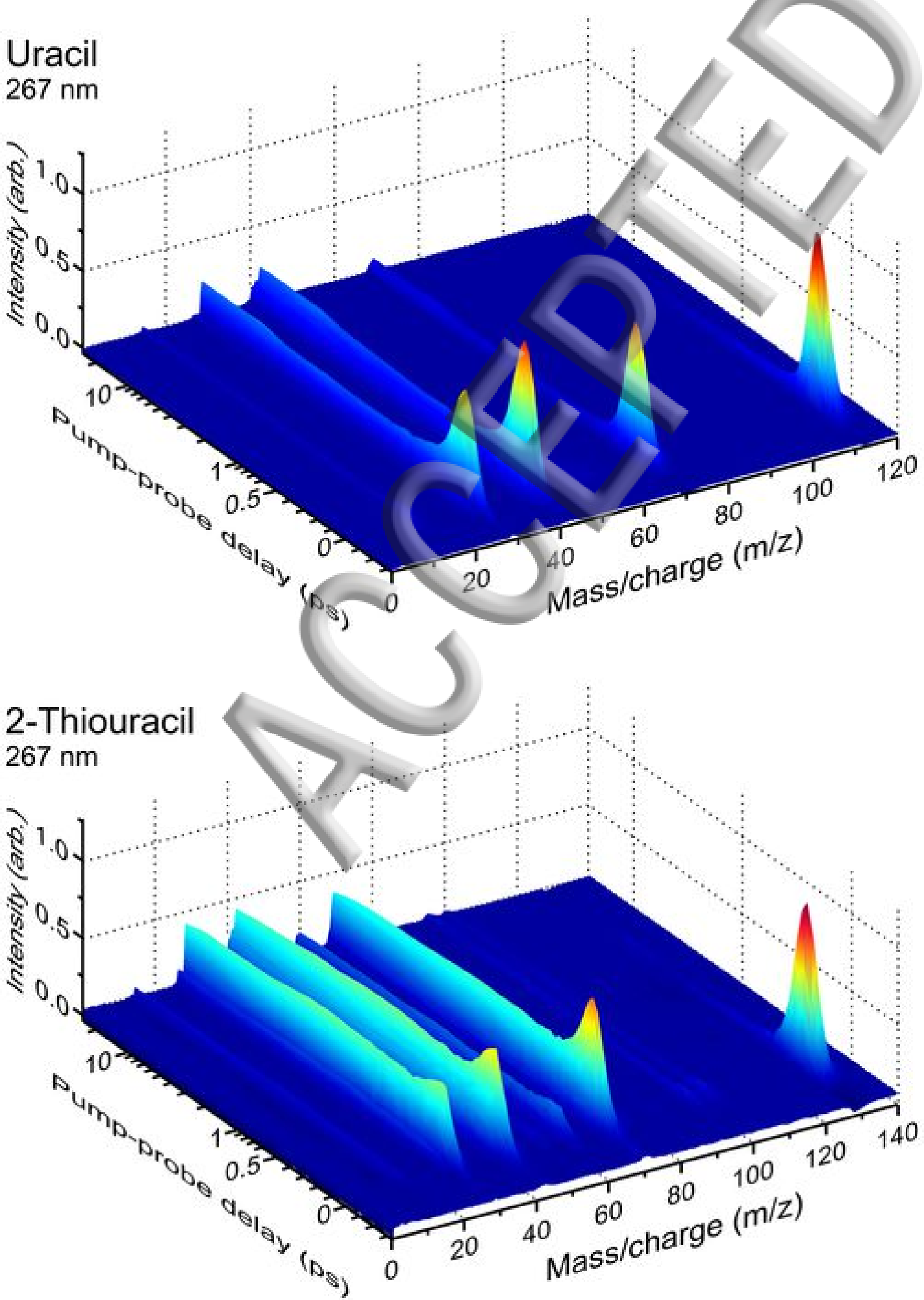
Uracil
267 nm
Intensity (arb.)
1.0
0.5
0.0
10
1
0.5
0
Pump-probe delay (ps)
0
20
40
60
80
100
120
Mass/charge (m/z)
2-Thiouracil
267 nm
Intensity (arb.)
1.0
0.5
0.0
10
1
0.5
0
Pump-probe delay (ps)
0
20
40
60
80
100
120
140
Mass/charge (m/z)

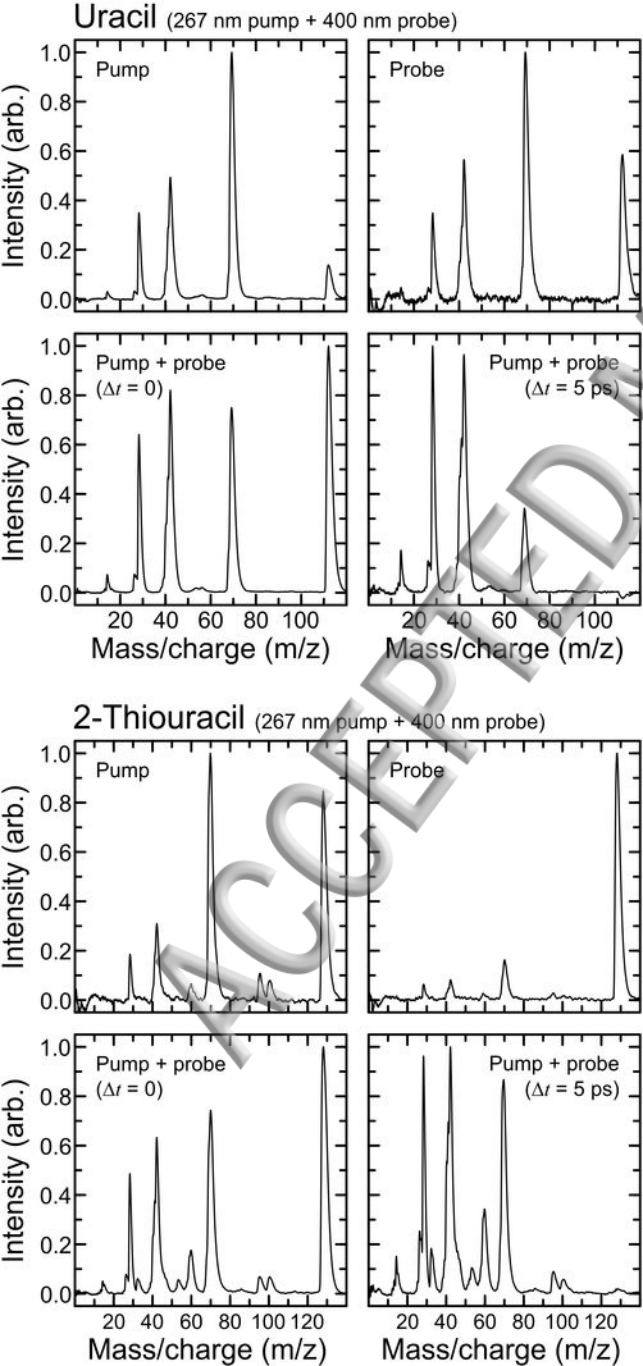
Uracil (267 nm pump + 400 nm probe)
Pump
Probe
Pump + probe
(Δt = 0)
Pump + probe
(Δt = 5 ps)
Intensity (arb.)
Mass/charge (m/z)
2-Thiouracil (267 nm pump + 400 nm probe)
Pump
Probe
Pump + probe
(Δt = 0)
Pump + probe
(Δt = 5 ps)
Intensity (arb.)
Mass/charge (m/z)

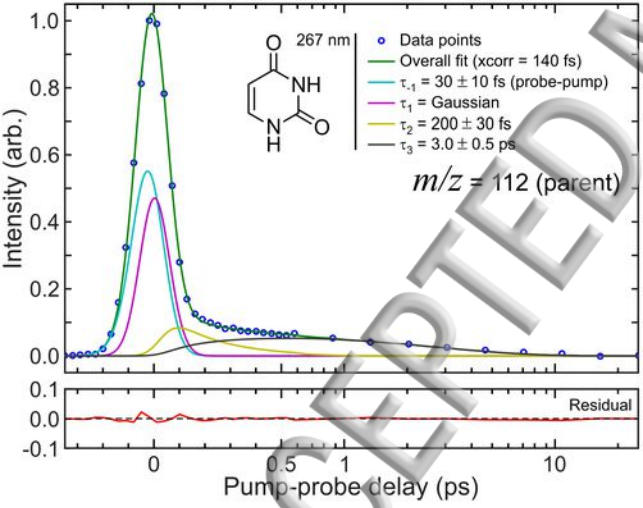
267 nm
Data points
Overall fit (xcorr = 140 fs)
τ-1 = 30 ± 10 fs (probe-pump)
τ1 = Gaussian
τ2 = 200 ± 30 fs
τ3 = 3.0 ± 0.5 ps
m/z = 112 (parent)
Intensity (arb.)
Residual
Pump-probe delay (ps)

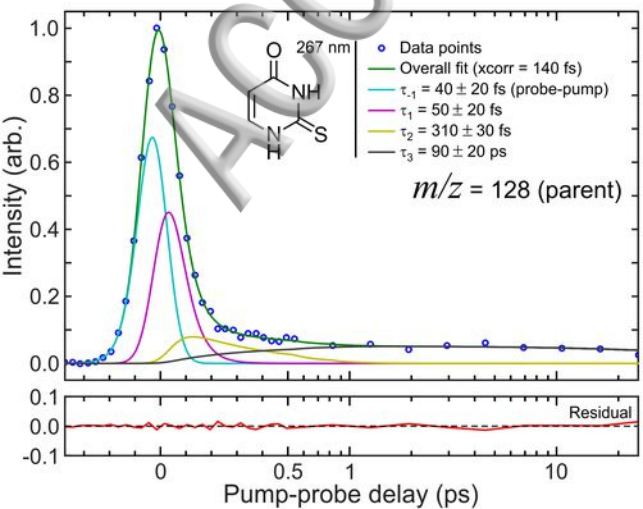
267 nm
Data points
Overall fit (xcorr = 140 fs)
τ-1 = 40 ± 20 fs (probe-pump)
τ1 = 50 ± 20 fs
τ2 = 310 ± 30 fs
τ3 = 90 ± 20 ps
m/z = 128 (parent)
Intensity (arb.)
Residual
Pump-probe delay (ps)

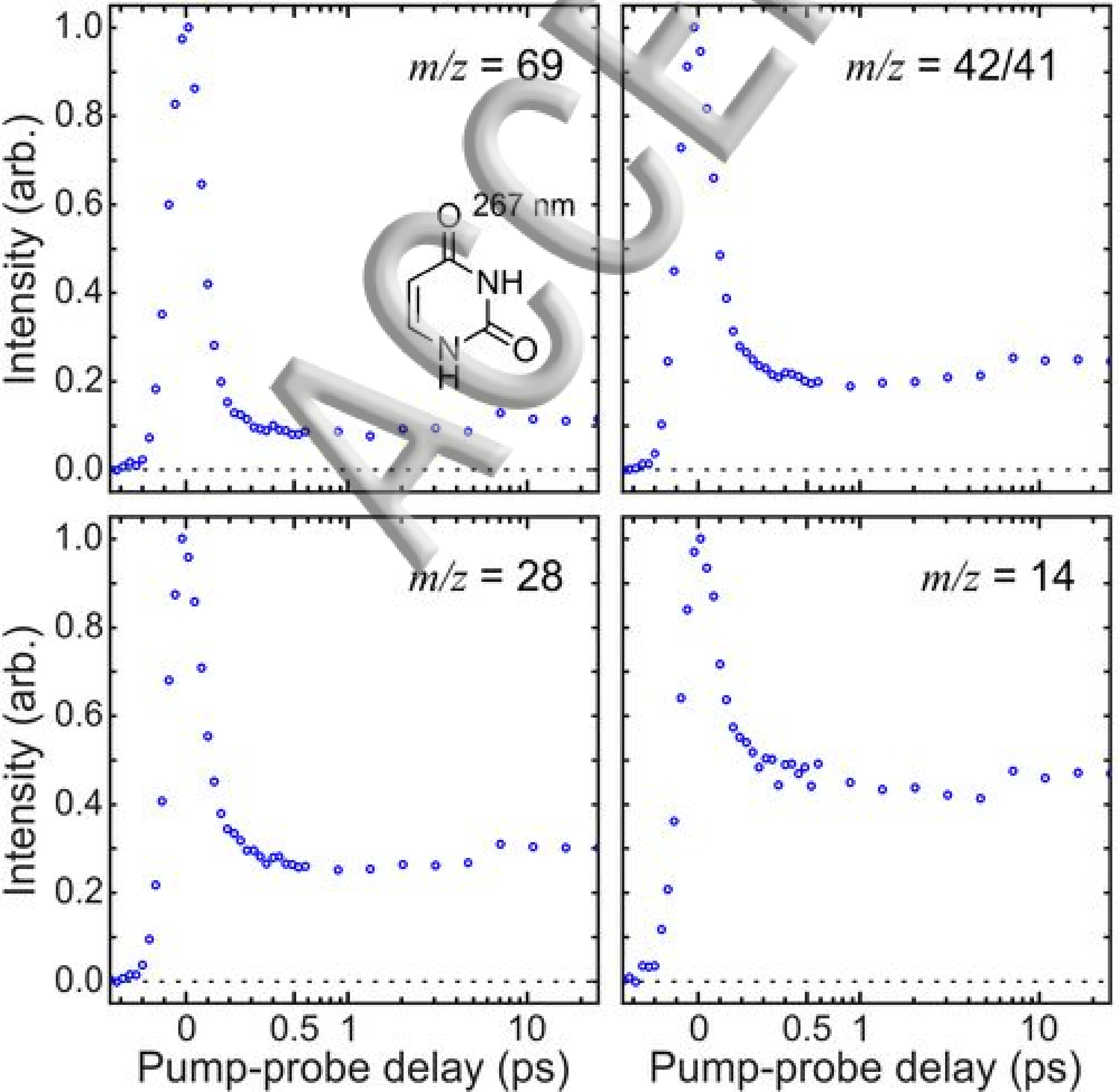
m/z = 69
m/z = 42/41
m/z = 28
m/z = 14
267 nm
O
NH
N
H
O
Intensity (arb.)
Intensity (arb.)
1.0
0.8
0.6
0.4
0.2
0.0
0
0.5
1
10
Pump-probe delay (ps)
Pump-probe delay (ps)

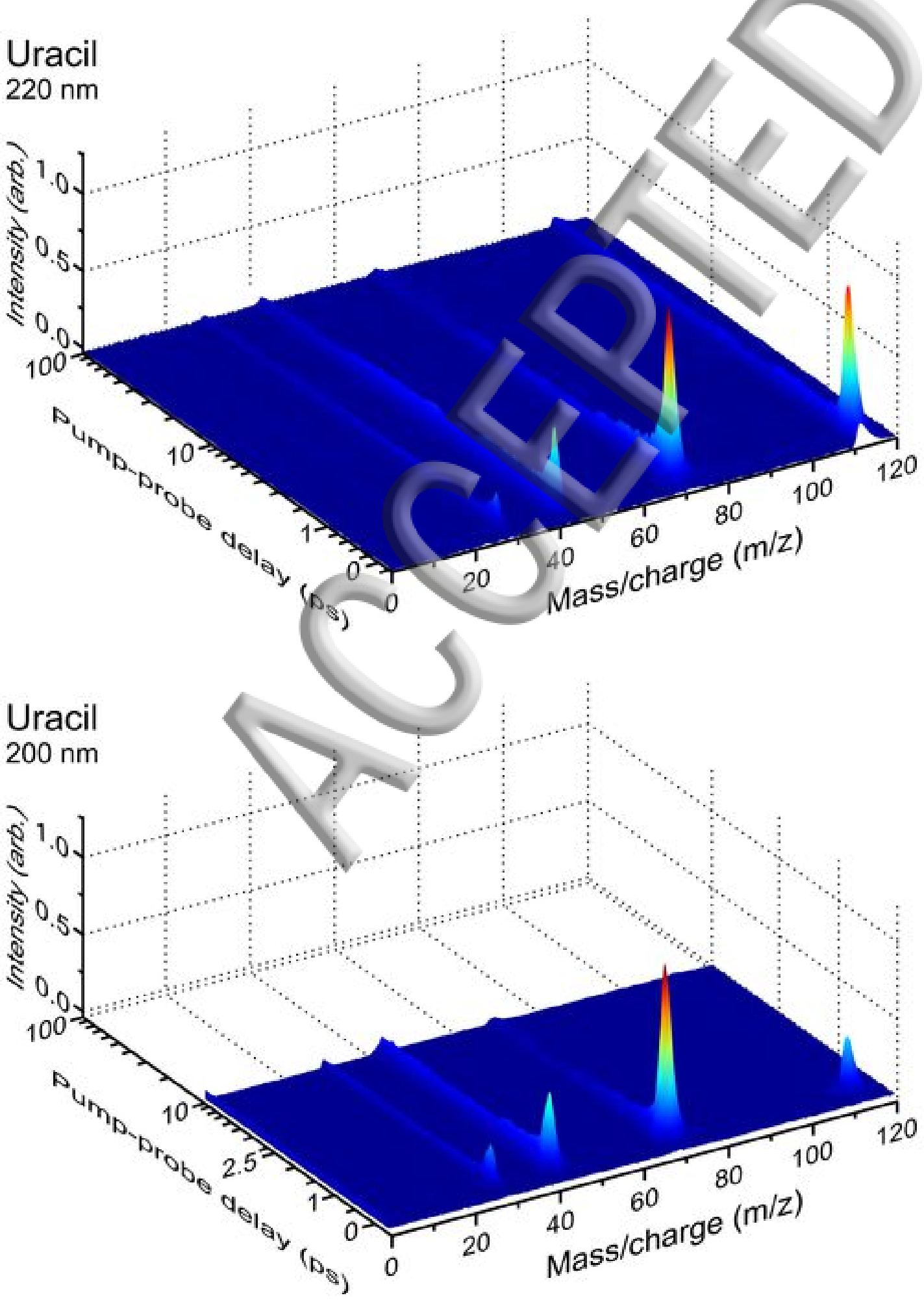
Uracil
220 nm
Intensity (arb.)
1.0
0.5
0.0
100
10
1
0
Pump-probe delay (ps)
0
20
40
60
80
100
120
Mass/charge (m/z)
Uracil
200 nm
Intensity (arb.)
1.0
0.5
0.0
100
10
2.5
1
0
Pump-probe delay (ps)
0
20
40
60
80
100
120
Mass/charge (m/z)

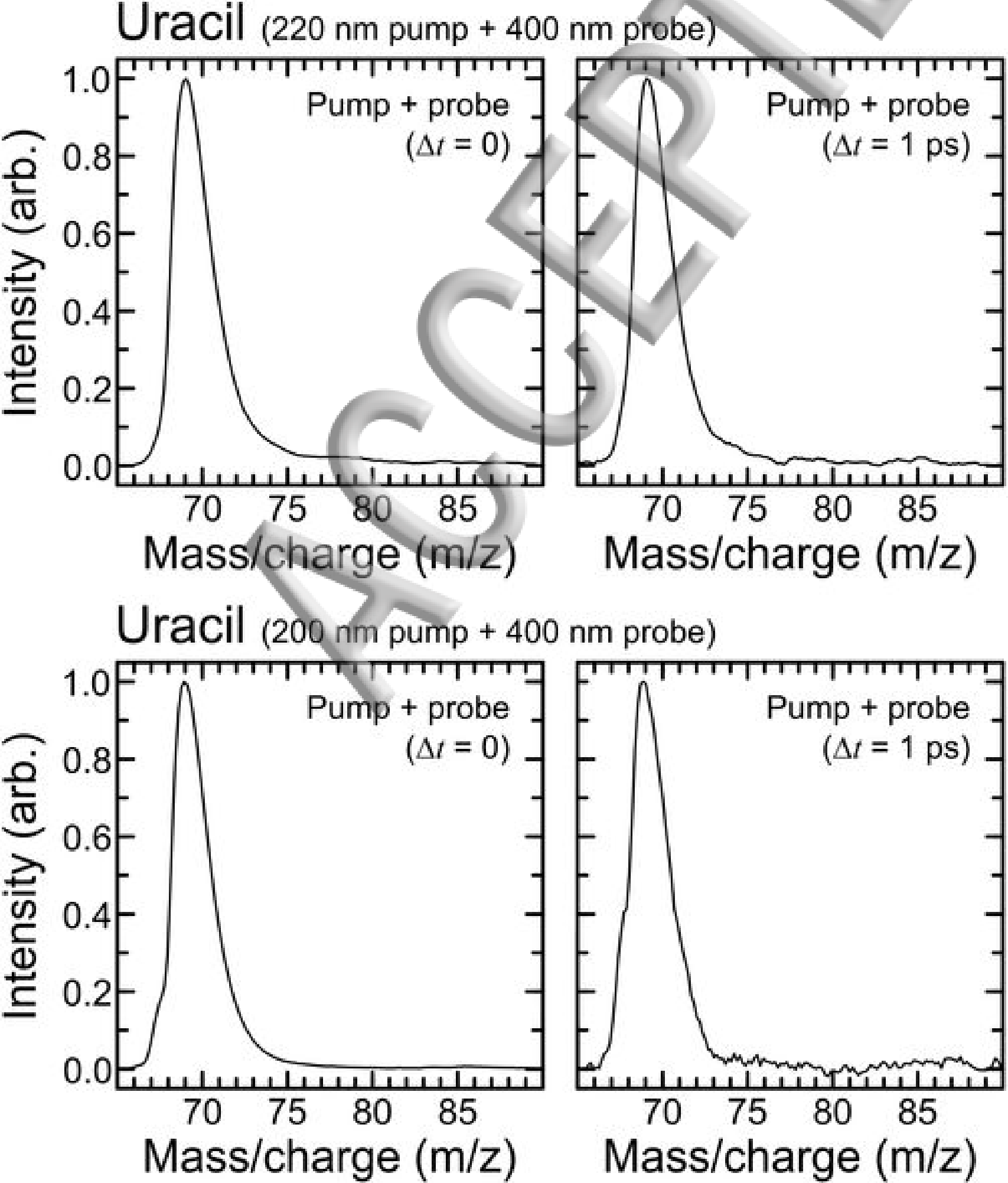
Uracil (220 nm pump + 400 nm probe)
Pump + probe
(Δt = 0)
Pump + probe
(Δt = 1 ps)
Intensity (arb.)
1.0
0.8
0.6
0.4
0.2
0.0
70
75
80
85
Mass/charge (m/z)
Uracil (200 nm pump + 400 nm probe)
Pump + probe
(Δt = 0)
Pump + probe
(Δt = 1 ps)
Intensity (arb.)
Mass/charge (m/z)

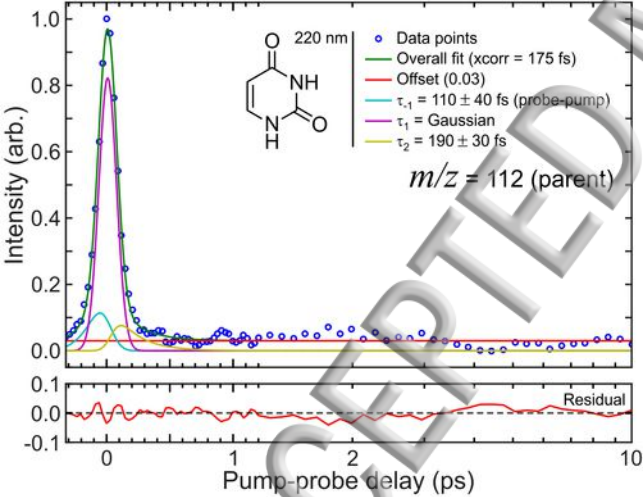
220 nm
Data points
Overall fit (xcorr = 175 fs)
Offset (0.03)
τ-1 = 110 ± 40 fs (probe-pump)
τ1 = Gaussian
τ2 = 190 ± 30 fs
m/z = 112 (parent)
Intensity (arb.)
Residual
Pump-probe delay (ps)

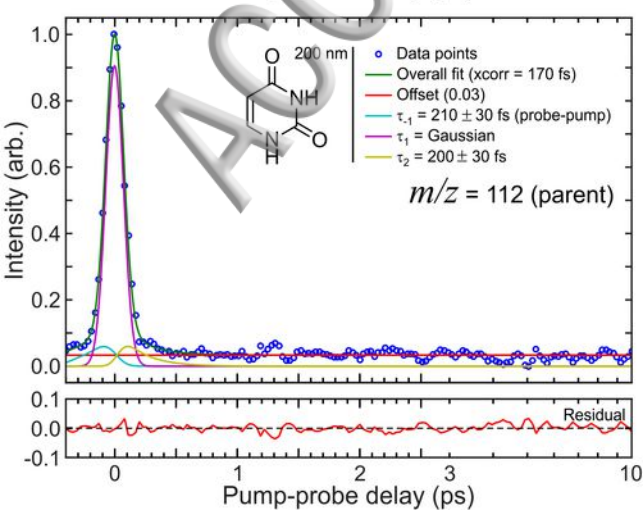
200 nm
Data points
Overall fit (xcorr = 170 fs)
Offset (0.03)
τ-1 = 210 ± 30 fs (probe-pump)
τ1 = Gaussian
τ2 = 200 ± 30 fs
m/z = 112 (parent)
Intensity (arb.)
Residual
Pump-probe delay (ps)

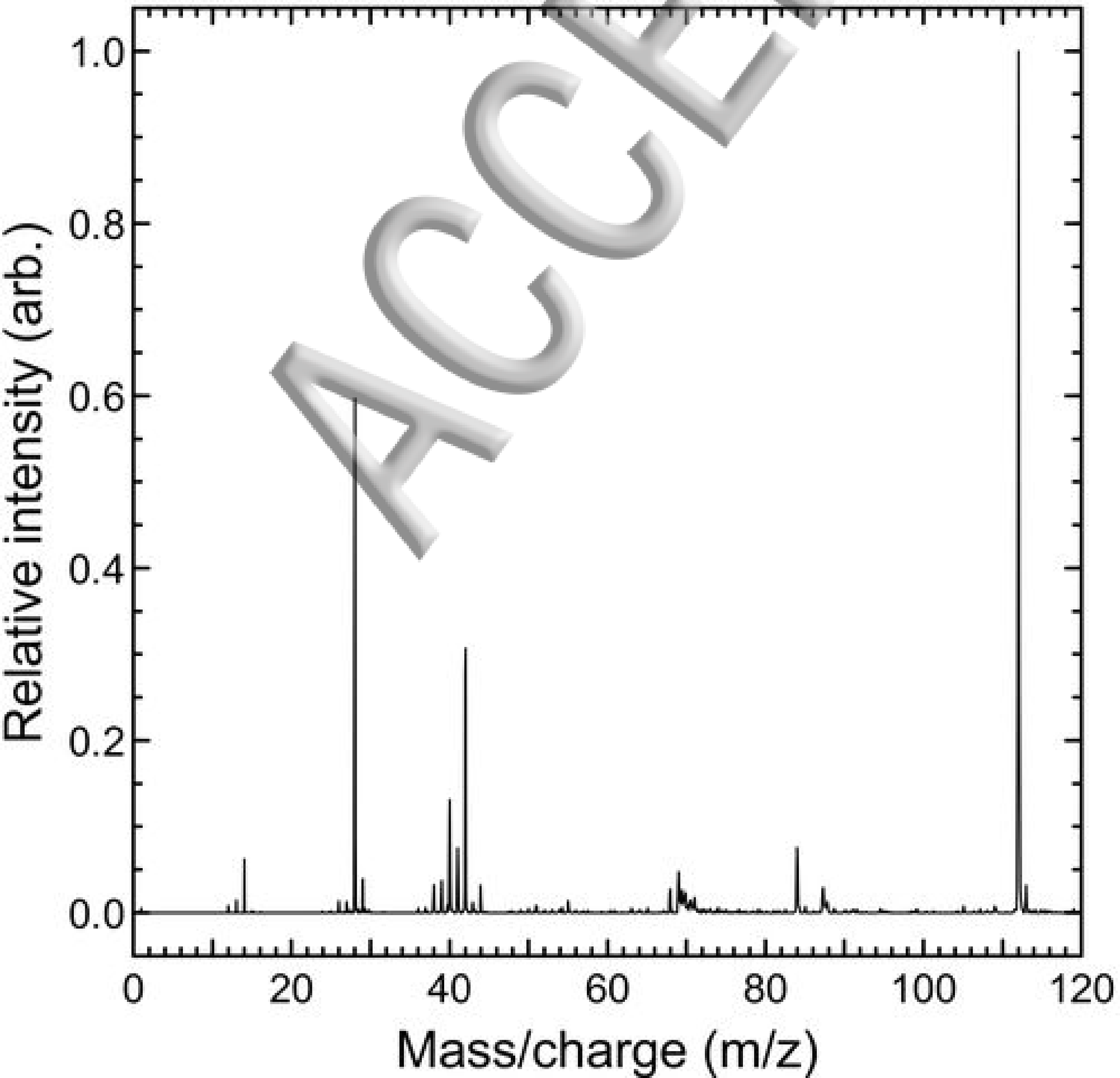
Relative intensity (arb.)
1.0
0.8
0.6
0.4
0.2
0.0
0
20
40
60
80
100
120
Mass/charge (m/z)

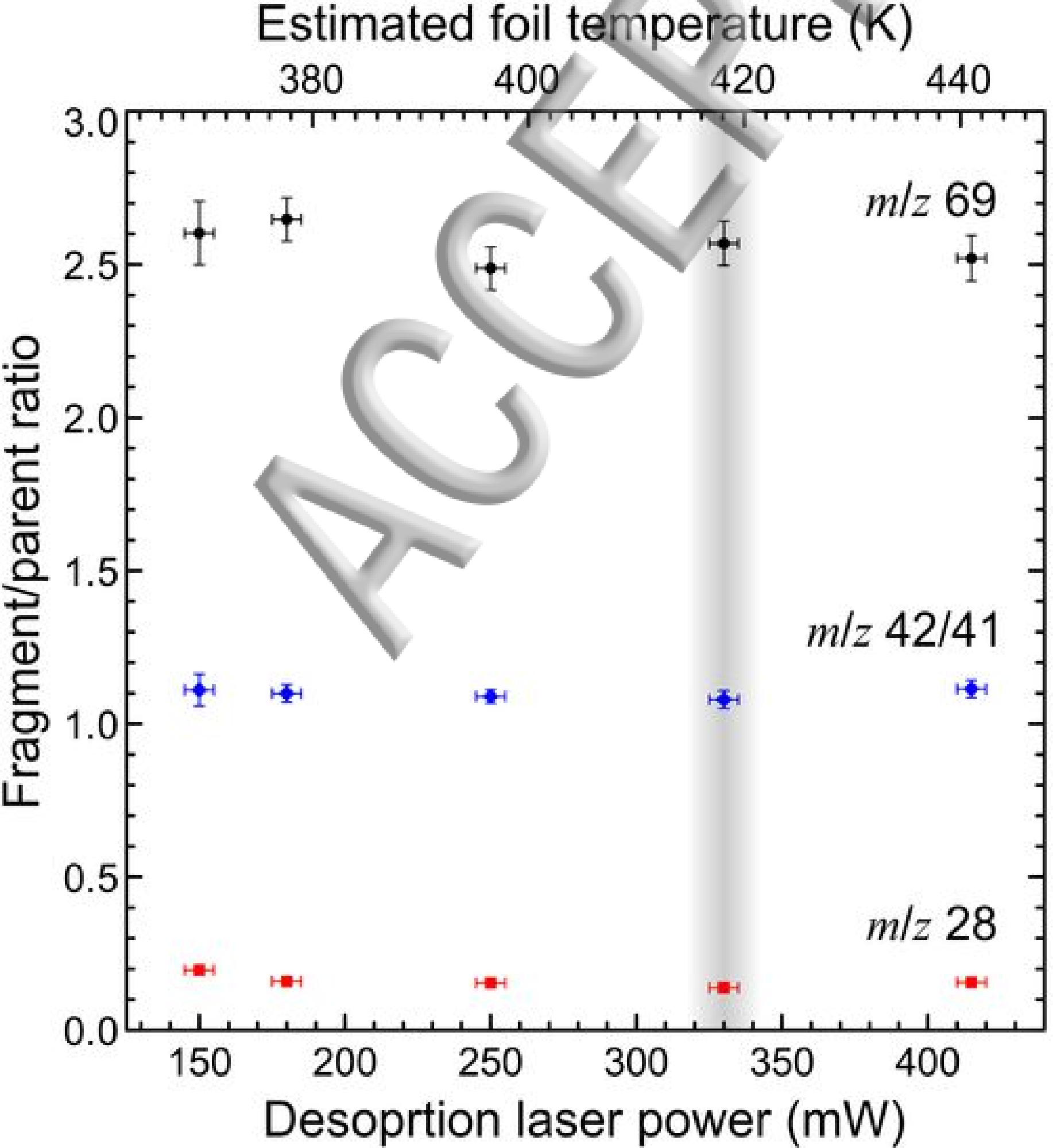
Estimated foil temperature (K)
380
400
420
440
3.0
2.5
2.0
1.5
1.0
0.5
0.0
Fragment/parent ratio
m/z 69
m/z 42/41
m/z 28
150
200
250
300
350
400
Desoprtion laser power (mW)

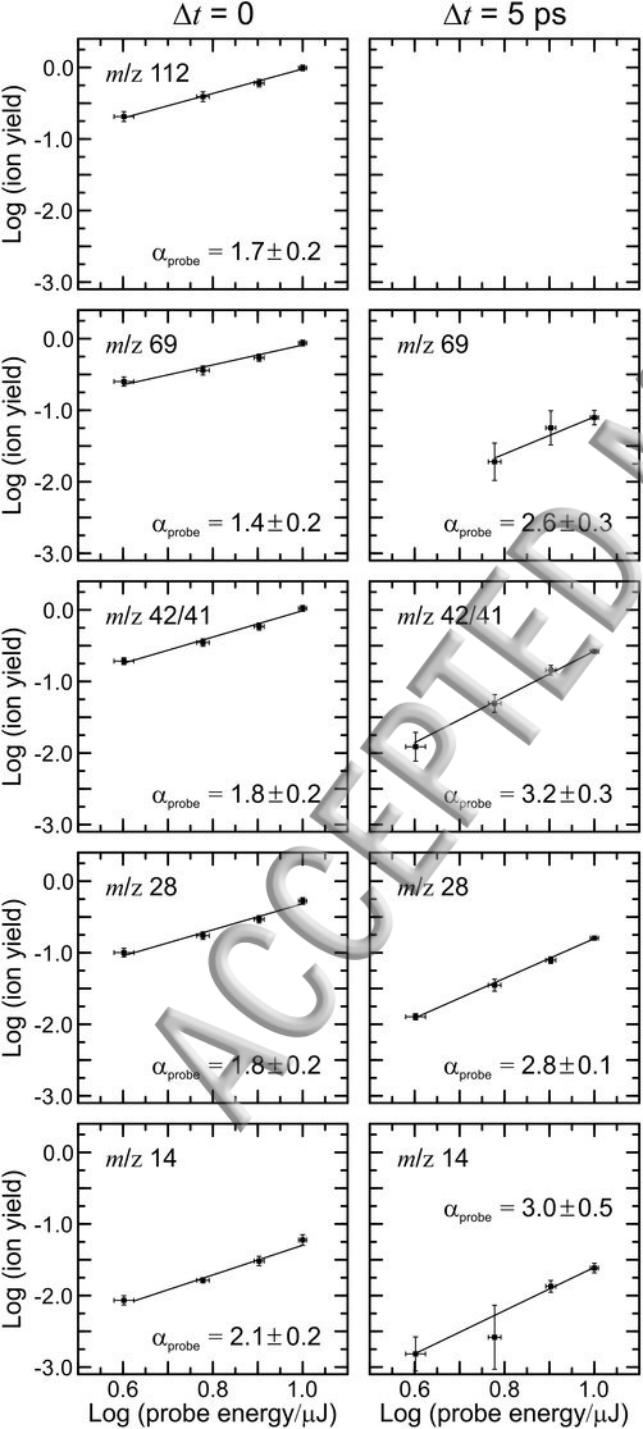
Δt = 0
Δt = 5 ps
m/z 112
m/z 69
m/z 69
m/z 42/41
m/z 42/41
m/z 28
m/z 28
m/z 14
m/z 14
Log (ion yield)
0.0
-1.0
-2.0
-3.0
α_probe = 1.7±0.2
α_probe = 1.4±0.2
α_probe = 2.6±0.3
α_probe = 1.8±0.2
α_probe = 3.2±0.3
α_probe = 1.8±0.2
α_probe = 2.8±0.1
α_probe = 2.1±0.2
α_probe = 3.0±0.5
0.6
0.8
1.0
Log (probe energy/μJ)